# Impacts of bromine and iodine chemistry on tropospheric OH and $HO_2$: Comparing observations with box and global model perspectives

**Daniel Stone,[1] Tomás Sherwen,[2] Mathew J. Evans,[2,3] Stewart Vaughan,[1] Trevor Ingham,[1,4] Lisa K. Whalley,[1,4] Peter M. Edwards,[2] Katie A. Read,[2,3] James D. Lee,[2,3] Sarah J. Moller,[2,3] Lucy J. Carpenter, [2,3] Alastair C. Lewis, [2,3] Dwayne E. Heard[1,4]**

[1] School of Chemistry, University of Leeds, Leeds, UK

[2] Wolfson Atmospheric Chemistry Laboratories, Department of Chemistry, University of York, York, UK

[3] National Centre for Atmospheric Science, University of York, York, UK

[4] National Centre for Atmospheric Science, University of Leeds, Leeds, UK

* Now at Department of Chemistry, University of York, York, UK

## Supplementary Material

## Speciation of modelled peroxy radicals

Figure S1 shows the speciation of peroxy radicals during SOS determined by the box model. The dominant species at Cape Verde are $HO_2$ and $CH_3O_2$, which comprise 87.4 % of the total peroxy radical concentration, and are followed by $CH_3C(O)O_2$ (6.5 %) and $C_2H_5O_2$ (1.1 %), all of which display no $HO_2$ interference in the laboratory (Whalley et al., 2013; Stone et al., 2014). Any peroxy species potentially contributing to interferences in $HO_2$ measurements thus constitutes < 4 % of the total peroxy radical concentration, with each species representing < 1 % of the total. Potential interferences arising from conversion of alkene- and aromatic-derived peroxy radicals to OH within the LIF detection cell, as described by Fuchs et al. (2011), are thus expected to be small for SOS and are not explicitly described in the model for this work.

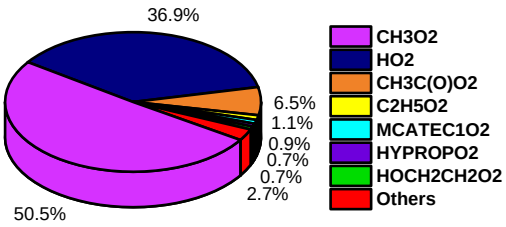


Figure S1: Speciation of peroxy radicals during SOS1 and SOS2. Radical names are as given by the MCM.

## Impact of $CH_3O_2$ + OH

Recent experiments have indicated a rapid reaction between $CH_3O_2$ and OH (Bossolasco et al., 2014; Fittschen et al., 2014; Assaf et al., 2016; Yan et al., 2016), with the dominant products expected to be $CH_3O$ + $HO_2$ at an observed yield of (0.8 ± 0.2) (Assaf et al., 2017). As shown in Figures 5 and 6 (main text), this reaction contributes 4 %, on average, to the total midday OH loss during SOS and 5 % to the total $HO_2$ production, assuming 100 % yield of $CH_3O$ + $HO_2$. Inclusion of the reaction in the chemistry scheme, for model runs in which halogens are included, decreases the modelled concentration of OH at midday from 5.3 $\times 10^6$ $cm^{-3}$ to 5.2 $\times 10^6$ $cm^{-3}$, and increases the $HO_2$ concentration from 3.2 $\times 10^8$ $cm^{-3}$ to 3.9 $\times 10^8$ $cm^{-3}$.

Figure S2 shows the mean modelled diurnal profile for $CH_3O_2$ during SOS, for model runs with and without the reaction between $CH_3O_2$ and OH. Inclusion of the reaction decreases the mean midday $CH_3O_2$ concentration by 24 %, from 5.7 $\times 10^8$ $cm^{-3}$ to 4.6 $\times 10^8$ $cm^{-3}$, and thus has a more significant impact on $CH_3O_2$ than on OH or $HO_2$. Similar changes to modelled OH, $HO_2$ and $CH_3O_2$ were reported by Assaf et al. (2017) using an updated MCM based model for the RHaMBLe campaign in Cape Verde in 2007 (Whalley et al., 2010).

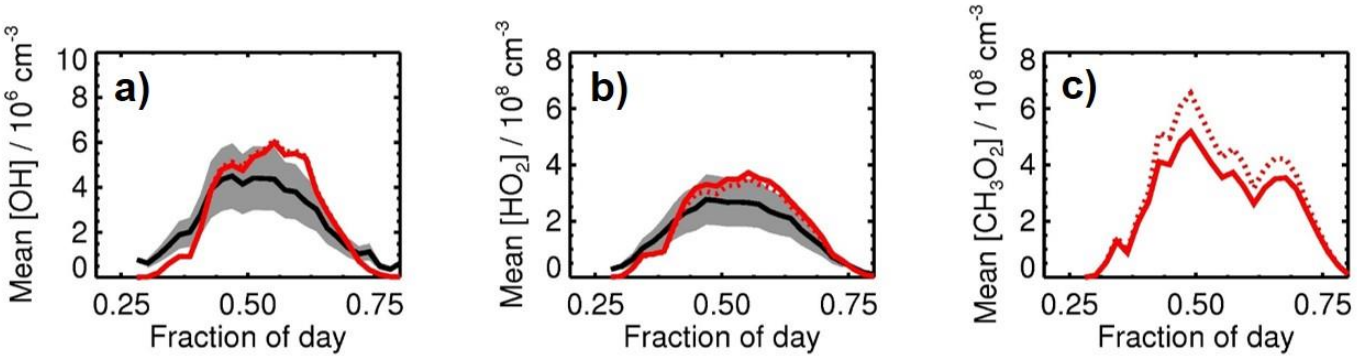


Figure S2: Mean box modelled diurnal profiles for a) OH; b) $HO_2$; c) $CH_3O_2$ during SOS (SOS1 and SOS2 combined) for model runs with (red solid line) and without (red broken line) the reaction between $CH_3O_2$ and OH. For OH and $HO_2$, observations are shown in black, with grey shading indicating the variability in the observations.

Figure S3 shows the mean midday (1100 to 1300 hours) budgets for $CH_3O_2$ during SOS for model runs with and without the reaction between $CH_3O_2$ and OH. Midday production of $CH_3O_2$, both with and without the reaction between $CH_3O_2$ and OH, is dominated by $CH_3$ radical production from $CH_4$ + OH (~ 55 %), and is followed by the reactions of $CH_3C(O)O_2$ radicals with NO (~ 17 %) and other $RO_2$ radicals (~ 15 %). Midday loss of $CH_3O_2$, when $CH_3O_2$ is included, is dominated by reactions with NO (~ 41 %), $HO_2$ (~ 33 %), the reaction with OH (~ 15 %), and $CH_3O_2$ self-reaction (~ 8 %). If the reaction of $CH_3O_2$ with OH is not included in the model, the loss

reaction with NO represents ~ 48 % of the total $CH_3O_2$ loss and the reactions with $HO_2$ and other $CH_3O_2$ radicals represent ~ 36 % and ~ 12 %, respectively.

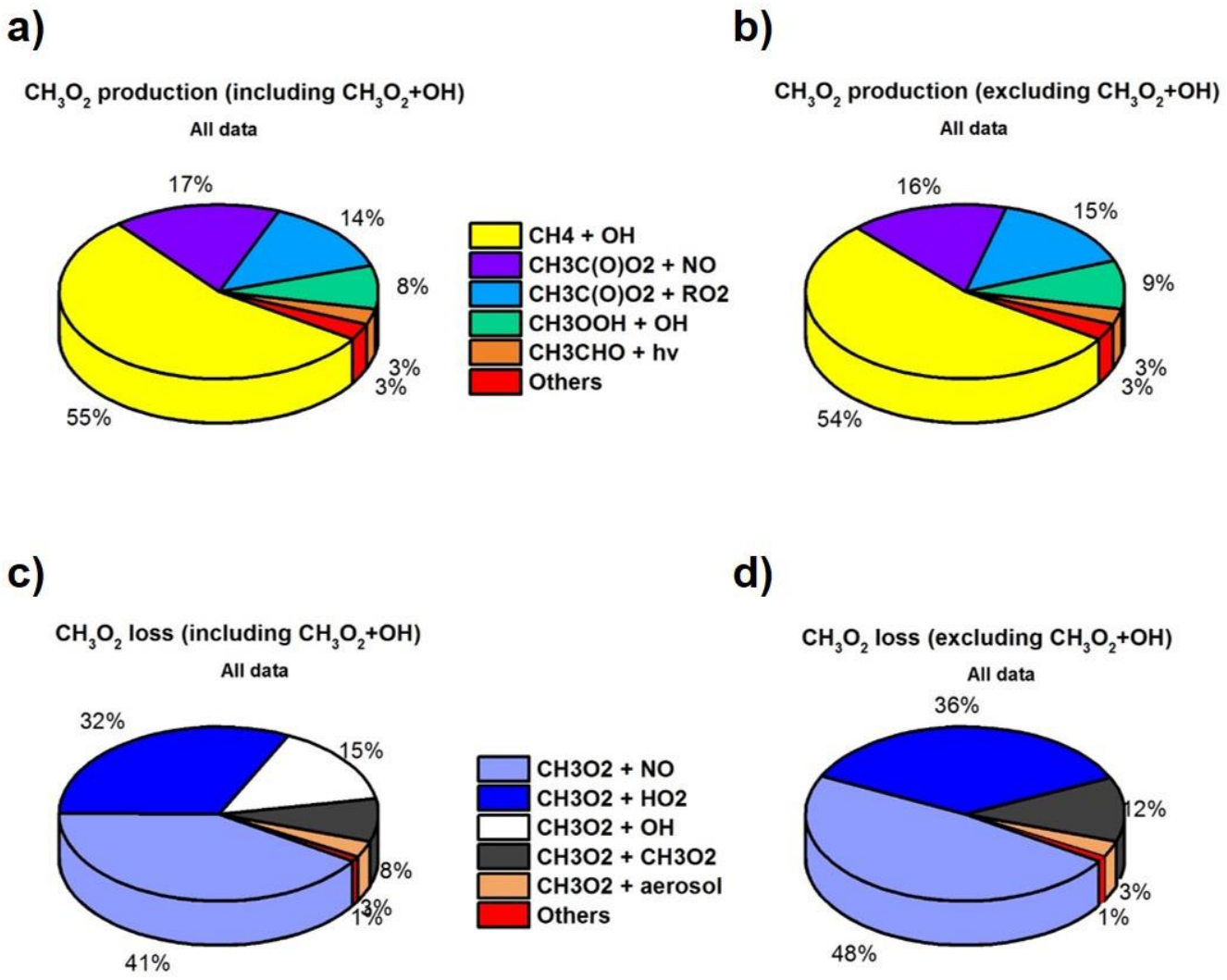


Figure S3: Mean midday (1100 to 1300 hours) budgets for $CH_3O_2$ during SOS (SOS1 and SOS2 combined). Panel a) production of $CH_3O_2$ for model runs with the reaction between $CH_3O_2$ and OH; b) production of $CH_3O_2$ for model runs without the reaction between $CH_3O_2$ and OH; c) loss of $CH_3O_2$ for model runs with the reaction between $CH_3O_2$ and OH; d) loss of $CH_3O_2$ for model runs without the reaction between $CH_3O_2$ and OH.

## Time series for observed and box modelled OH and $HO_2$ radical concentrations

Figures S4 and S5 shows the times series for OH and $HO_2$ observations and model simulations day-by-day during SOS1 and SOS2.

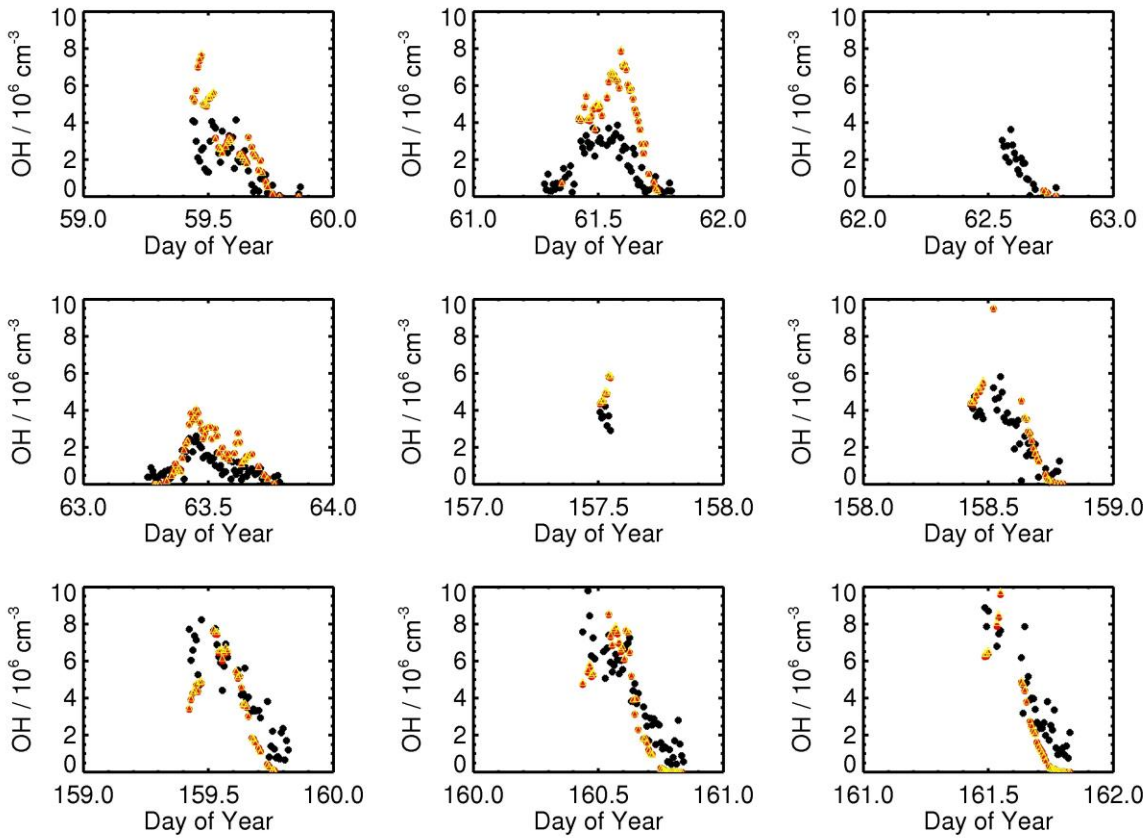


Figure S4: Times series for observed and modelled OH during SOS1 (days 59 to 63) and SOS2 (days 157 to 162). Observed data are shown in black; box model concentrations with halogen chemistry are shown by filled red circles; box model concentrations without halogen chemistry are shown by open yellow triangles.

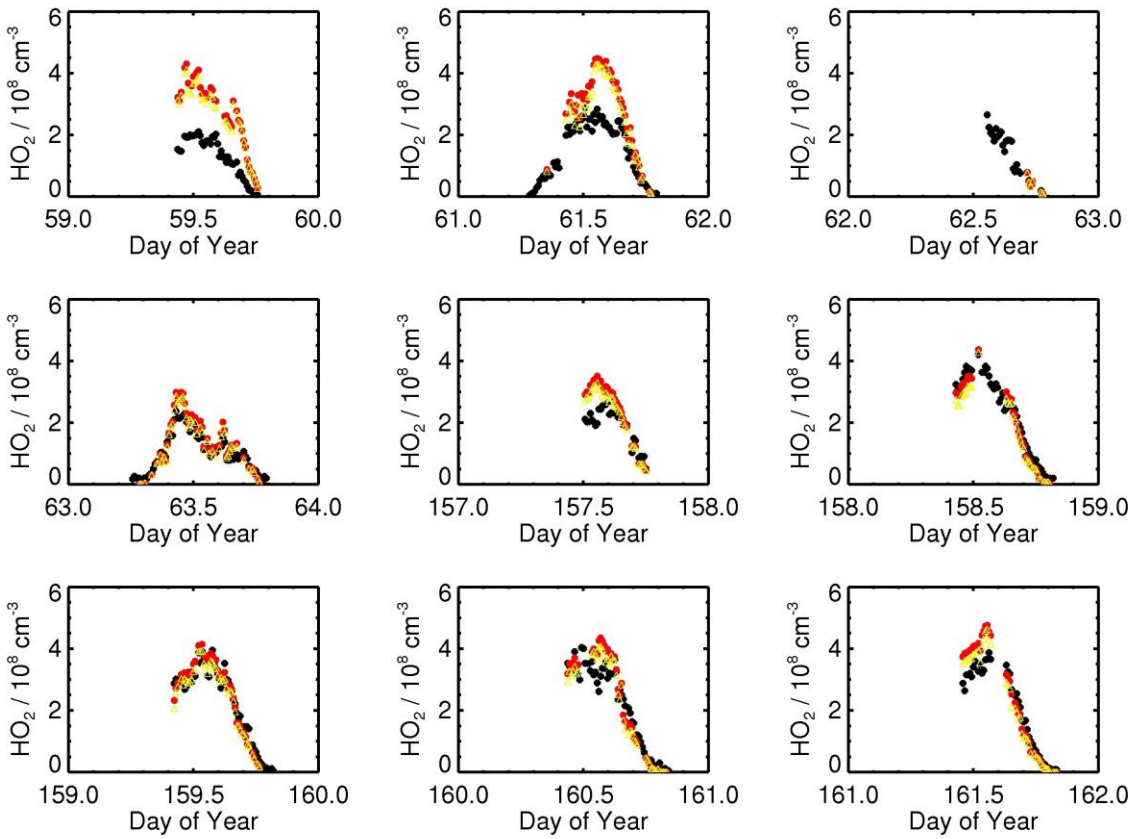


Figure S5: Times series for observed and modelled $HO_2$ during SOS1 (days 59 to 63) and SOS2 (days 157 to 162). Observed data are shown in black; box model concentrations with halogen chemistry are shown by filled red circles; box model concentrations without halogen chemistry are shown by open yellow triangles.

## Box model sensitivity of OH and $HO_2$ to BrO and IO mixing ratios

Observations of BrO and IO at the Cape Verde Atmospheric Observatory show average diurnal mixing ratios of 2.5 ppt and 1.4 ppt, respectively, which were used as constraints in the box model simulations presented in this work. In order to test the sensitivity of OH and $HO_2$ to these constraints, we have performed simulations in which the BrO and IO mixing ratios were constrained to the upper and lower limits of the observed values (3.5 ppt and 1.5 ppt for BrO and 2.0 ppt and 1.0 ppt for IO, as reported by Read et al. (2008) and Mahajan et al. (2010)). In addition, simulations were performed in which mixing ratios of BrO and IO increase from 0600 hours and reach the constant values of 2.5 ppt and 1.4 ppt, respectively, as shown by Read et al. (2008). Results from these simulations are shown in Figure S6, and indicate that there are only minor differences in the OH and $HO_2$ concentrations between simulations performed on constraining to the upper and lower limits of the observed BrO

and IO concentrations, and that there is little sensitivity of OH or $HO_2$ to the early morning mixing ratios of BrO and IO.

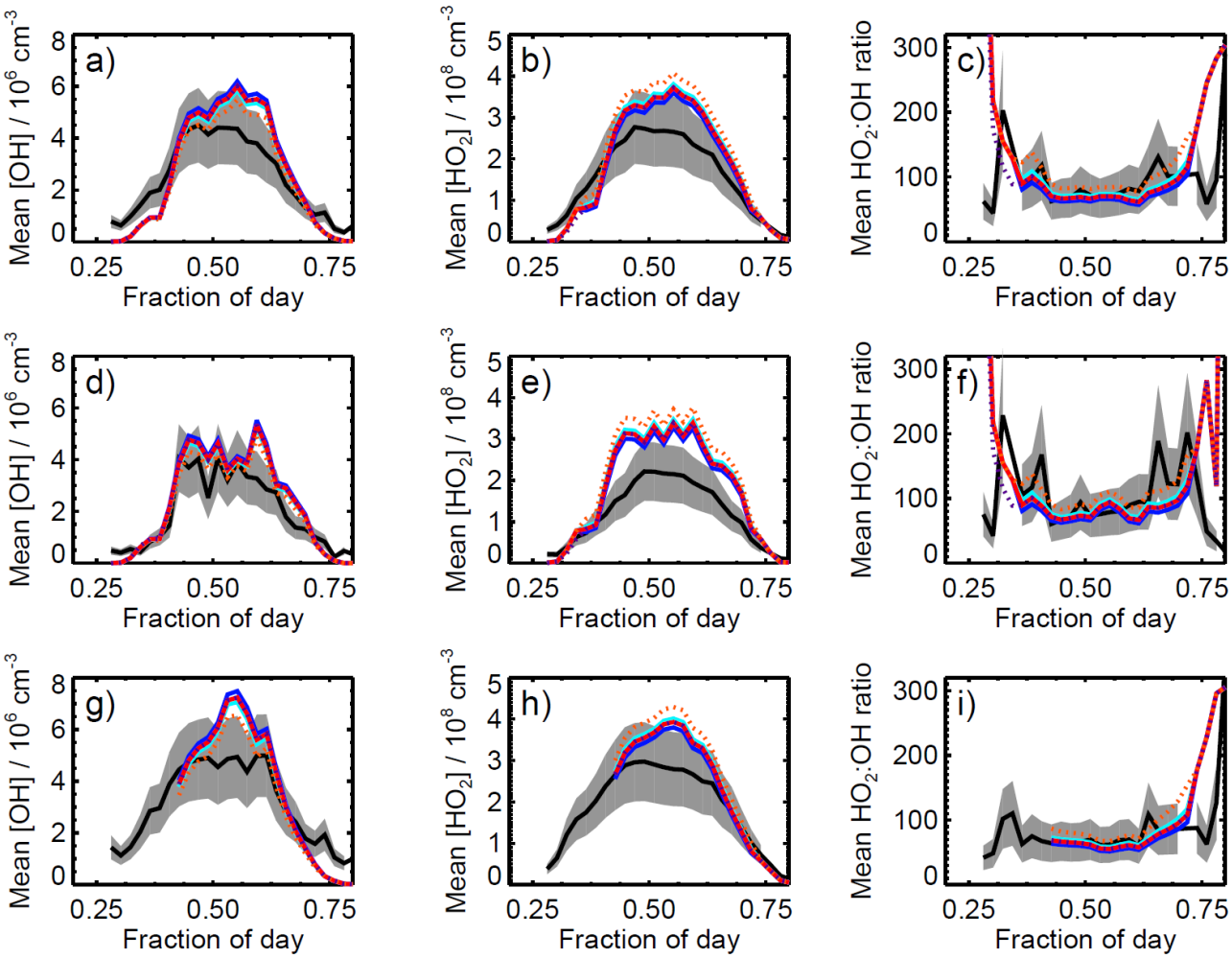


Figure S6: Impacts of changes to BrO and IO constraints on average diurnal profiles for a) OH during both measurement periods; b) $HO_2$ during both measurement periods; c) $HO_2$:OH ratio during both measurement periods; d) OH during SOS1 (Feb-Mar 2009); e) $HO_2$ during SOS1; f) $HO_2$:OH during SOS1; g) OH during SOS2 (May-June); h) $HO_2$ during SOS2; i) $HO_2$:OH ratio during SOS2. Observed data are shown in black, with grey shading indicating the variability in the observations; model simulations constrained to the average daytime (0930 to 1830 hours) mixing ratios of BrO (2.5 ppt) and IO (1.4 ppt) are shown in red; simulations constrained to the upper limits to the daytime mixing ratios of BrO (3.5 ppt) and IO (2.0 ppt) are shown in dark blue; simulations constrained to the lower limits to the daytime mixing ratios of BrO (1.5 ppt) and IO (1.0 ppt) are shown in light blue; simulations constrained to the average daytime mixing ratios of BrO (2.5 ppt) and IO (1.4 ppt) and including increases in the mixing ratios from 0600 hours are shown by the dashed purple lines; simulations with no halogens are shown by the dashed orange lines.

## References


Assaf, E., Song, B., Tomas, A., Schoemaker, C., and Fittschen, C.: Rate constant of the reaction between $CH_3O_2$ and OH radicals revisited, J. Phys. Chem. A, 120, 8923-8932, 2016

Assaf, E., Sheps, L., Whalley, L., Heard, D., Tomas, A., Schoemaecker, C., and Fittschen, C.: The reaction between $CH_3O_2$ and OH radicals: Product yields and atmospheric implications, Environ. Sci. Technol., 51, 4, 2170-2177, doi: 10.1021/acs.est.6b06265, 2017

Bossolasco, A., Farago, E.P., Schoemaker, C., and Fittschen, C.: Rate constant of the reaction between $CH_3O_2$ and OH radicals, Chem. Phys. Lett., 593, 7-13, 2014

Fittschen, C., Whalley, L.K., and Heard, D.E.: The reaction of $CH_3O_2$ radicals with OH radicals: A neglected sink for $CH_3O_2$ in the remote atmosphere, Environ. Sci. Technol., 118, 7700-7701, 2014

Fuchs, H., Bohn, B., Hofzumahaus, A., Holland, F., Lu, K. D., Nehr, S., Rohrer, F., Wahner, A.: Detection of $HO_2$ by laser induced fluorescence: calibration and interferences from $RO_2$ radicals, Atmos. Meas. Tech., 4, 1209–1225, 2011

Mahajan, A.S., Plane, J.M.C., Oetjen, H., Mendes, L., Saunders, R.W., Saiz-Lopez, A., Jones, C.E., Carpenter, L.J., McFiggans, G.B.: Measurement and modelling of tropospheric reactive halogen species over the tropical Atlantic Ocean, Atmos. Chem. Phys., 10, 4611-4624, 2010

Read, K. A., Mahajan, A. S., Carpenter, L. J., Evans, M. J., Faria, B. V. E., Heard, D. E., Hopkins, J. R., Lee, J. D., Moller, S. J., Lewis, A. C., Mendes, L., McQuaid, J. B., Oetjen, H., Saiz-Lopez, A., Pilling, M. J., Plane, J. M. C.: Extensive halogen mediated ozone destruction over the tropical Atlantic Ocean, Nature, 453, 7199, 1232–1235, 2008

Stone, D., Evans, M.J., Walker, H., Ingham, T., Vaughan, S., Ouyang, B., Kennedy, O.J., McLeod, M.W., Jones, R.L., Hopkins, J., Punjabi, S., Lidster, R., Hamilton, J.F., Lee, J.D., Lewis, A.C., Carpenter, L.J., Forster, G., Oram, D..E., Reeves, C.E., Bauguitte, S., Morgan, W., Coe, H., Aruffo, E., Dari-Salisburgo, C., Giammaria, F., Di Carlo, P., and Heard, D.E.: Radical Chemistry at Night: Comparisons between observed and modeled $HO_x$, $NO_3$ and $N_2O_5$ during the RONOCO project, Atmos. Chem. Phys., 14, 1299-1321, 2014, doi:10.5194/acp-14-1299-2014

Whalley, L.K., Furneaux, K.L., Goddard, A., Lee, J.D., Mahajan, A., Oetjen, H., Read, K.A., Kaaden, N., Carpenter, L.J., Lewis, A.C., Plane, J.M.C., Saltzman, E.S., Wiedensohler, A., Heard, D.E.: The chemistry of OH and $HO_2$ radicals in the boundary layer over the tropical Atlantic Ocean, Atmos. Chem. Phys., 10, 1555-1576, 2010

Whalley, L.K., Blitz, M.A., Desservettaz, M., Seakins, P.W., and Heard, D.E.: Reporting the sensitivity of laser-induced fluorescence instruments used for $HO_2$ detection to an interference from $RO_2$ radicals and introducing a novel approach that enables $HO_2$ and certain $RO_2$ types to be selectively measured, Atmos. Meas. Tech., 6, 3425-3440, 2013, doi:10.5194/amt-6-3425-2013

Yan, C., Kocevska, S., and Krasnoperov, L.N.: Kinetics of the reaction of $CH_3O_2$ radicals with OH studied over the 292-526 K temperature range, J. Phys. Chem. A, 120, 6111-6121, 2016